Supplementary Information: *In-situ* electric field X-ray total scattering reveals composition-dependent electromechanical strain mechanisms in $(1-x)\mathbf{BiFe_{2/8}Ti_{3/8}Mg_{3/8}O_3} - x\mathbf{PbTiO_3}$ ceramics

Brooke N. Richtik,[a] Rachel Beall,[b] Leah Bellcase,[b] Vedika Shah,[b] Tiffany L. Kinnibrugh,[c] Simon Trudel,*[a] Jacob L. Jones, and Michelle R. Dolgos*[a,d]

[a] *Department of Chemistry, University of Calgary, 2500 University Dr NW, Calgary, AB, T2N 1N4 Canada.*
[b] *Department of Materials Science and Engineering, North Carolina State University, Raleigh, NC 27695 USA.*
[c] *Advanced Photon Source, Argonne National Laboratory 9700 S Cass Ave, Lemont, IL 60439, USA.*
[d] *Oak Ridge National Laboratory, 1 Bethel Valley Rd, Oak Ridge, TN 37830, USA.*

* E-mail: dolgosmr@ornl.gov; trudels@ucalgary.ca

CONTENTS

S1 Field Emission Scanning Electron Microscopy

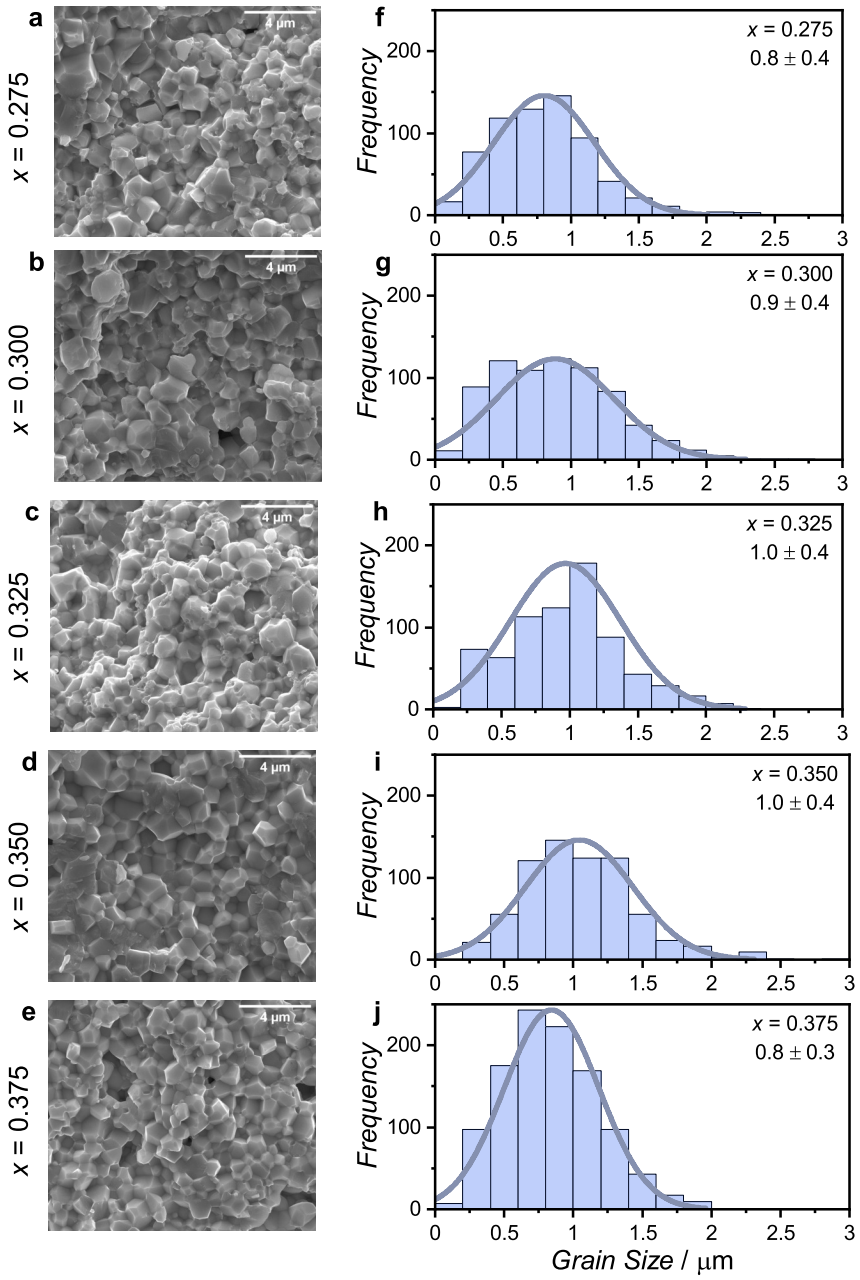

Fig. S1 (a-e) Cross-sectional field emission scanning electron microscopy (FESEM) images of BFTM-xPT(x = 0.275-0.375) ceramics. Images were collected on a fractured ceramic bar coated with Pt using an FESEM (FEI Quanta FEG 250) with the accelerating voltage of 20 kV under high vacuum ($< 10^{-6}$ Torr). (f-j) Grain size distributions of BFTM-xPT(x = 0.275-0.375) ceramics. The average and standard deviation of grain sizes for each composition are shown (top right). Grain sizes were measured from three images taken from different regions of each fractured ceramic.

S2 Modeling the Pseudocubic Phase with Cc

Previous work (considering neutron diffraction data) concluded that the pseudocubic phase in BFTM-xPT (x = 0.300-0.325) is best described by space group *Cc*. To avoid over-refinement of x-ray diffraction data, modeled the pseudocubic phase with space group $R3m$ in this study. For completeness, we have included the Rietveld analysis using $R3m$+$P4mm$ to model the experiment data. The R_{wp} (%) of the texture refinements using this model are included in Table S1. Selected regions (111_{pc} and 002_{pc}) of the experimental data and calculated model are compared in Figure S2

Table S1 R_{wp} (%) values at different applied electric fields for the Rietveld refinements against X-ray diffraction data collected on BFTM-xPT (x=0.300 and 0.325) using a mixed-phase model with space groups *Cc* and *P4mm*. Here the psuedocubic phase is represented by space group *Cc*.

Applied Field (kV mm^{-1})	**x=0.300**	**x=0.325**
0	-	9.22
1	11.37	9.24
2	11.36	9.27
3	11.32	9.28
4	11.10	9.24
5	10.48	9.11
6	9.39	9.17
7	9.42	9.29
8	9.88	9.45
6 (down)	9.88	9.47
4 (down)	9.61	9.42
2 (down)	9.35	9.45
0 (down)	9.22	9.41

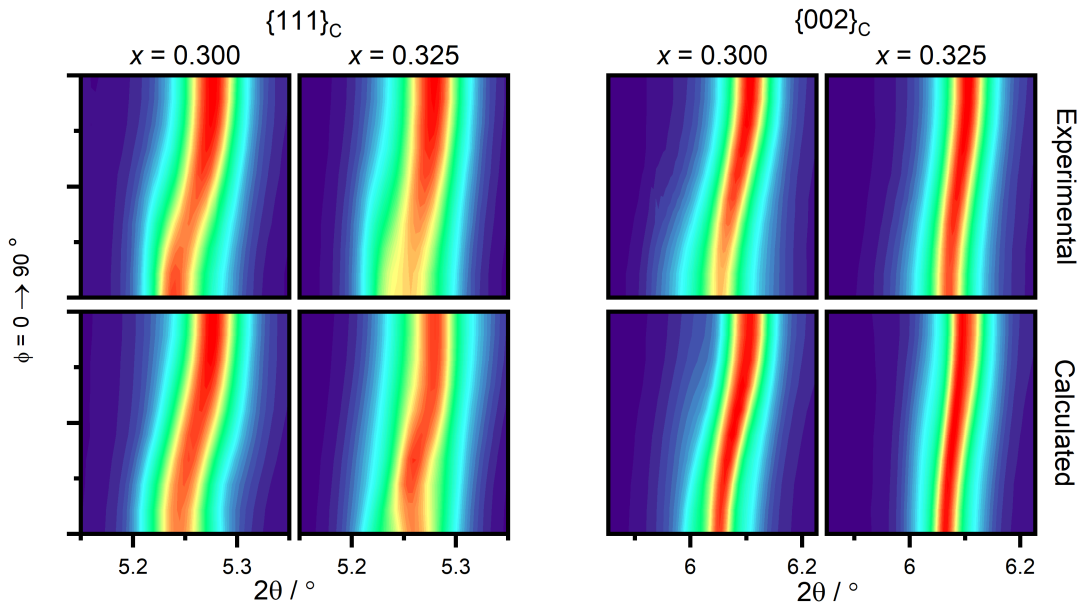

Fig. S2 δr gradient with linear fit to the high field linear region, the slope of each fit is reported for each composition.

The calculated 001 pole figure for the tetragonal phase, and the 111 pole figure for the pseudocubic phase from the *Cc*+*P*4*mm* model are shown in S3. The pseudocubic phase displays texture in compositions x=0.300 and 0.325. The strain originating from domain wall motion in the tetragonal phase was calculated by eqn. 3, and the strain from domain wall motion in the monoclinic phase was calculated by the following equation:

$$s_{33}^{\text{non-180}} = \frac{d_{111} - d_{11\bar{1}}}{d_{11\bar{1}}} \frac{1}{2\pi} \int_{\phi=0}^{\pi/2} \Delta f_{hkl^*}(\phi) \cdot \cos^2\phi \cdot \sin\phi \mathrm{d}\phi$$

where, Δf_{hkl^*} represents the change in pole figure direction ($f_{hkl^*_{E\neq 0}}$ - $f_{hkl^*_{E0}}$), ϕ denotes the angle with respect to the direction of the electric field, and the $\frac{d_{111}-d_{11\bar{1}}}{d_{11\bar{1}}}$ term accounts to the rhombohedral unit cell distortion. In space group *Cc*, the $(111)_{pc}$ and the $(11\bar{1})_{pc}$ reflections correspond to the $(002)_{pc}$ and $(40\bar{2})_{pc}$ reflections, respectively. The calculated strain from domain wall motion is shown in Figure S4. Despite having a high m.r.d. value, the strain originating from domain wall motion in *Cc*is small (0.03 %) due to a low distortion index. Thus, even with modeling the diffraction data with space group *Cc*, the majority of the strain still originates for intrinsic mechanisms within the MPB.

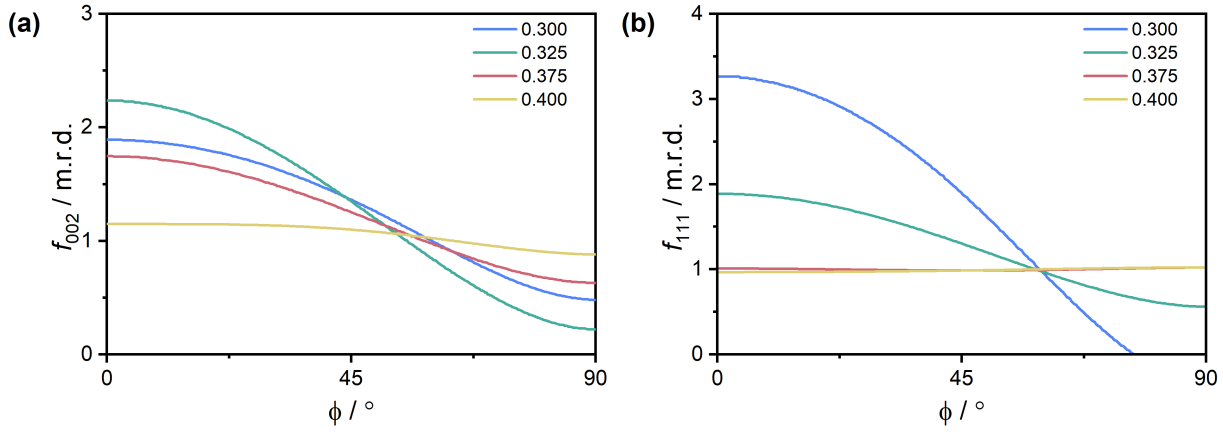

Fig. S3 Pole figures of BFTM-xPT obtained from Rietveld refinements against x-ray diffraction data. Where the refinements used a mixed-phase model with space groups *Cc*+*P*4*mm*. (a) 002 pole figures calculated from the tetragonal phase (space group *P*4*mm*). (b) 111 pole figure calculated from the pseudocubic phase (space group *Cc*)

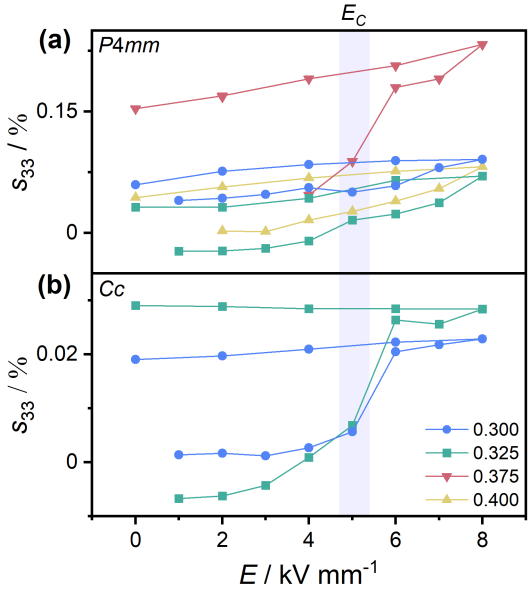

Fig. S4 (a) The non-180 °strain (s_{33}) from tetragonal phase (space group *P*4*mm*) domain wall motion in BFTM-xPT (x=0.300-0.400). (b) The non-180 °strain (s_{33}) from pseudocubic phase (space group *Cc*) domain wall motion in BFTM-xPT (x=0.300-0.325)

S3 Remanent Diffraction Data

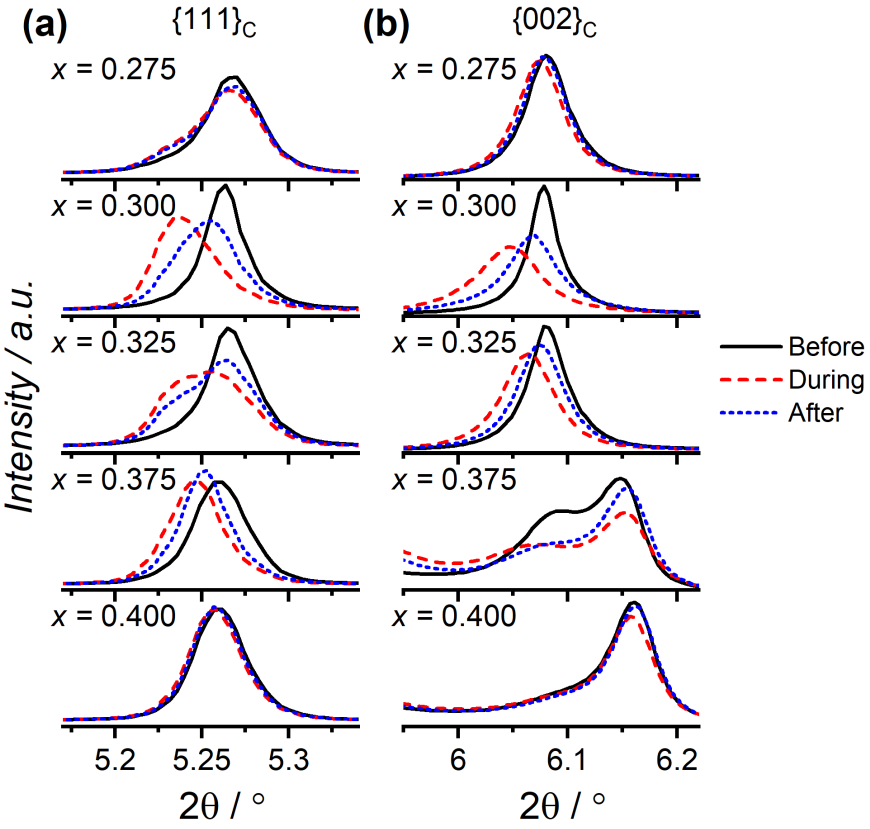

Fig. S5 Diffraction data collected before, during (at $8\,\mathrm{kV\,mm^{-1}}$), and after poling where the $(111)_{pc}$ and $(002)_{pc}$ family of reflections are shown in (a) and (b), respectively. Data were collected at $\lambda = 0.2116\,\text{Å}$, and $\phi = 0\,°$.

S4 Texture Refinements

The crystallographic parameters obtained from the refinement against ambient field data are reported in table S2. Structure from Richtik *et al.*[19] served as a starting model for these fits. Oxygen anion sites and isotropic displacement parameters (B_{eq}) for space group $P4mm$ were constrained to previous values[19]. For space group $R3m$, the oxygen anion B_{eq} was fixed to 1.0 Å^2 as this value has not been previously reported and should not be reasonably refined in X-ray diffraction data due to the low scattering intensity of oxygen compared to the heavy cations in this system. The B_{eq} was fixed to 0.5 Å^2 due to potential chemical inhomogeneity between phases in the sample, as discussed in previous work.[19]. For simplicity, occupancy remained fixed to stoichiometry values. The crystallographic parameters were then fixed to these values for the subsequent texture refinement. The R_{wp} values for all texture refinements are reported in Table S3.

The calculated pole figures obtained from the Rietveld refinements upon increasing and decreasing voltage are shown in figures S6 and S6, for tetragonal and pseudocubic phases, respectively.

Table S2 Crystallographic parameters obtained from Rietveld refinements against synchrotron x-ray diffraction data of BFTM-xPT (x = 0.300-0.400). Data collected at ambient applied field (E = 0 kV mm^{-1} for x = 0.325 and 0.400 and E = 1 kV mm^{-1} for x = 0.300 and 0.375).

$PbTiO_3$ content:		x = 0.300		x = 0.325		x = 0.375		x = 0.400	
Space group		*R*3*m*	*P*4*mm*	*R*3*m*	*P*4*mm*	*R*3*m*	*P*4*mm*	*R*3*m*	*P*4*mm*
weight %		74.7(4)	25.3(2)	65.2(3)	34.8(2)	39.8(2)	60.2(2))	30.7(1)	69.3(1)
a (Å)		3.9617(1)	3.9484(2)	3.9601(0)	3.9468(1)	3.9598(1)	3.9174(1)	3.9578(1)	3.9077(1)
b (Å)		3.9617(0)	3.9484(2)	3.9601(0)	3.9468(1)	3.9598(1)	3.9174(1)	3.9578(1)	3.9077(1)
c (Å)		3.9617(0)	3.9886(4)	3.9601(0)	3.9835(2)	3.9598(1)	4.0560(1)	3.9578(1)	4.0773(1)
α (°)		89.99(3)	90	89.88(1)	90	90.00(6)	90	90.03(2)	90
Pb/Bi	occ	0.700/0.300		0.675/0.325		0.625/0.375		0.600/0.400	
	x	0	0	0	0	0	0	0	0
	y	0	1/4	0	1/4	0	1/4	0	1/4
	z	0	0	0	0	0	0	0	0
	B_{eq} (Å^2)	7.02(6)	0.52(3)	7.48(6)	0.86(2)	4.28(3)	2.87(2)	5.02(4)	3.41(1)
Fe/Ti/Mg	occ	0.175/0.563/0.263		0.169/0.578/0.253		0.156/0.609/0.234		0.150/0.625/0.225	
	x	1/2	1/2	1/2	1/2	1/2	1/2	1/2	1/2
	y	1/2	1/2	1/2	1/2	1/2	1/2	1/2	1/2
	z	1/2	0.5885(13)	1/2	0.5905(9)	1/2	0.5781(7)	1/2	0.5702(5)
	B_{eq} (Å^2)	0.5	0.5	0.5	0.5	0.5	0.5	0.5	0.5
O1	occ	1.0	1.0	1.0	1.0	1.0	1.0	1.0	1.0
	x	1/2	1/2	1/2	1/2	1/2	1/2	1/2	1/2
	y	1/2	1/2	1/2	1/2	1/2	1/2	1/2	1/2
	z	0	0.095	0	0.093	0	0.101	0	0.101
	B_{eq} (Å^2)	1.0	3.43	1.0	2.91	1.0	2.12	1.0	2.12
O2	occ	-	1.0	-	1.0	-	1.0	-	1.0
	x	-	0	-	0	-	0	-	0
	y	-	1/2	-	1/2	-	1/2	-	1/2
	z	-	0.600	-	0.598	-	0.611	-	0.611
	B_{eq} (Å^2)	-	3.43	-	2.91	-	2.12	-	2.12
Rwp (%)		12.097		10.465		9.294		7.359	

Table S3 R_{wp} (%) values at different applied electric fields for the Rietveld refinements against X-ray diffraction data collected on BFTM-xPT (x=0.300-0.375) using a mixed-phase model with space groups $R3m$ and $P4mm$. Here the psuedocubic phase is represented by space group $R3m$.

Applied Field (kV mm^{-1})	**x=0.300**	**x=0.325**	**x=0.375**	**x=0.400**
Increasing Field				
0	–	10.465	–	7.361
1	12.097	9.452	9.294	10.016
2	11.681	9.485	9.072	10.010
3	11.634	9.517	8.857	10.006
4	11.422	9.521	9.028	10.027
5	10.773	9.461	9.105	10.014
6	9.710	9.558	10.082	10.042
7	9.931	9.717	10.233	10.040
8	10.578	10.402	10.715	10.069
Decreasing Field				
6	10.614	10.485	10.601	9.987
4	10.260	10.307	10.532	9.935
2	9.908	10.134	10.465	9.927
0	9.722	9.902	10.419	9.927

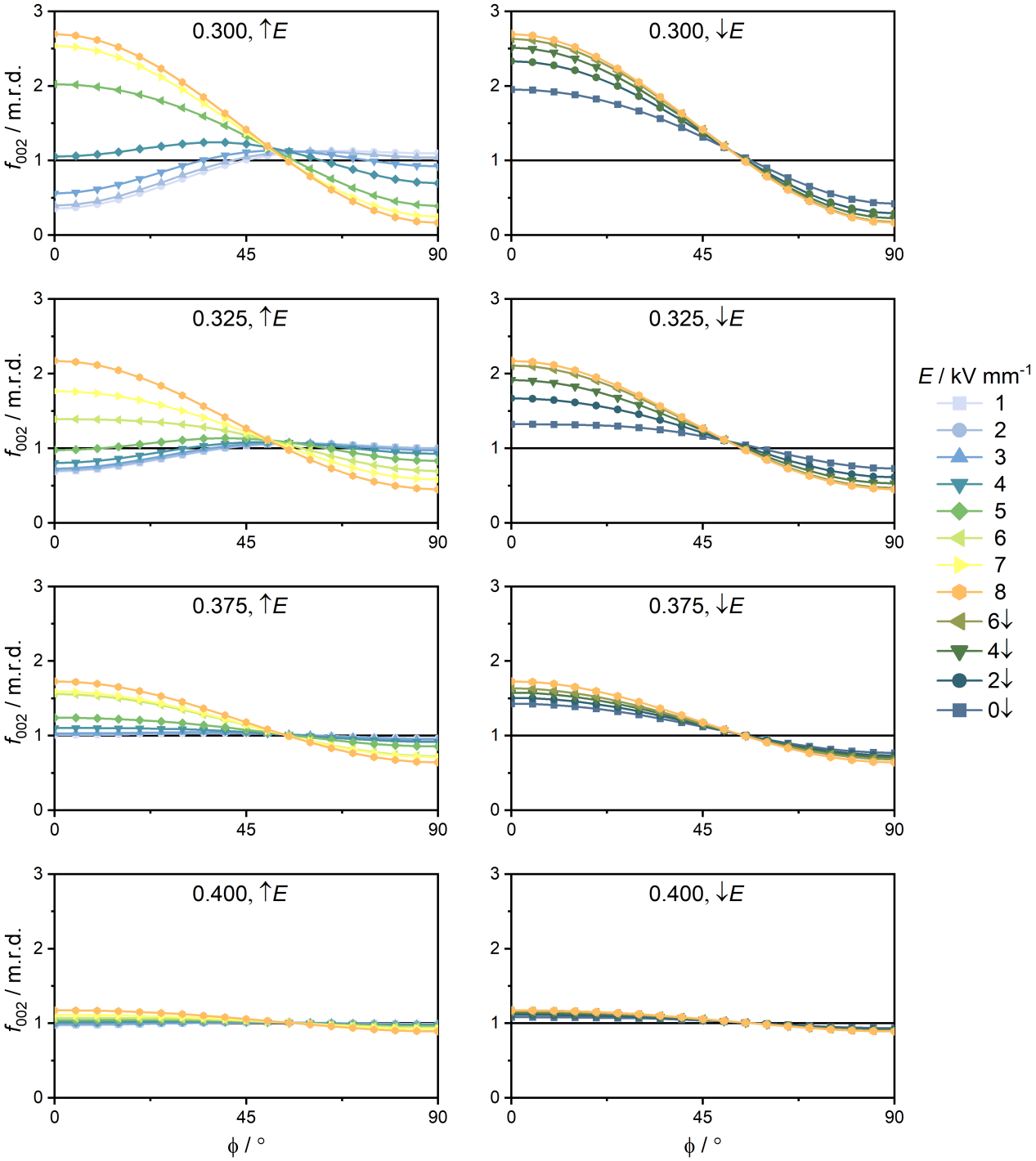

Fig. S6 Calculated 001 pole figures from the tetragonal (s.g. *P*4*mm*) phase in BFTM-*x*PT (*x*=0.300-0.375). Pole figures calculated from the Rietveld refinements where texture was modeled using a spherical harmonics model (order = 4).

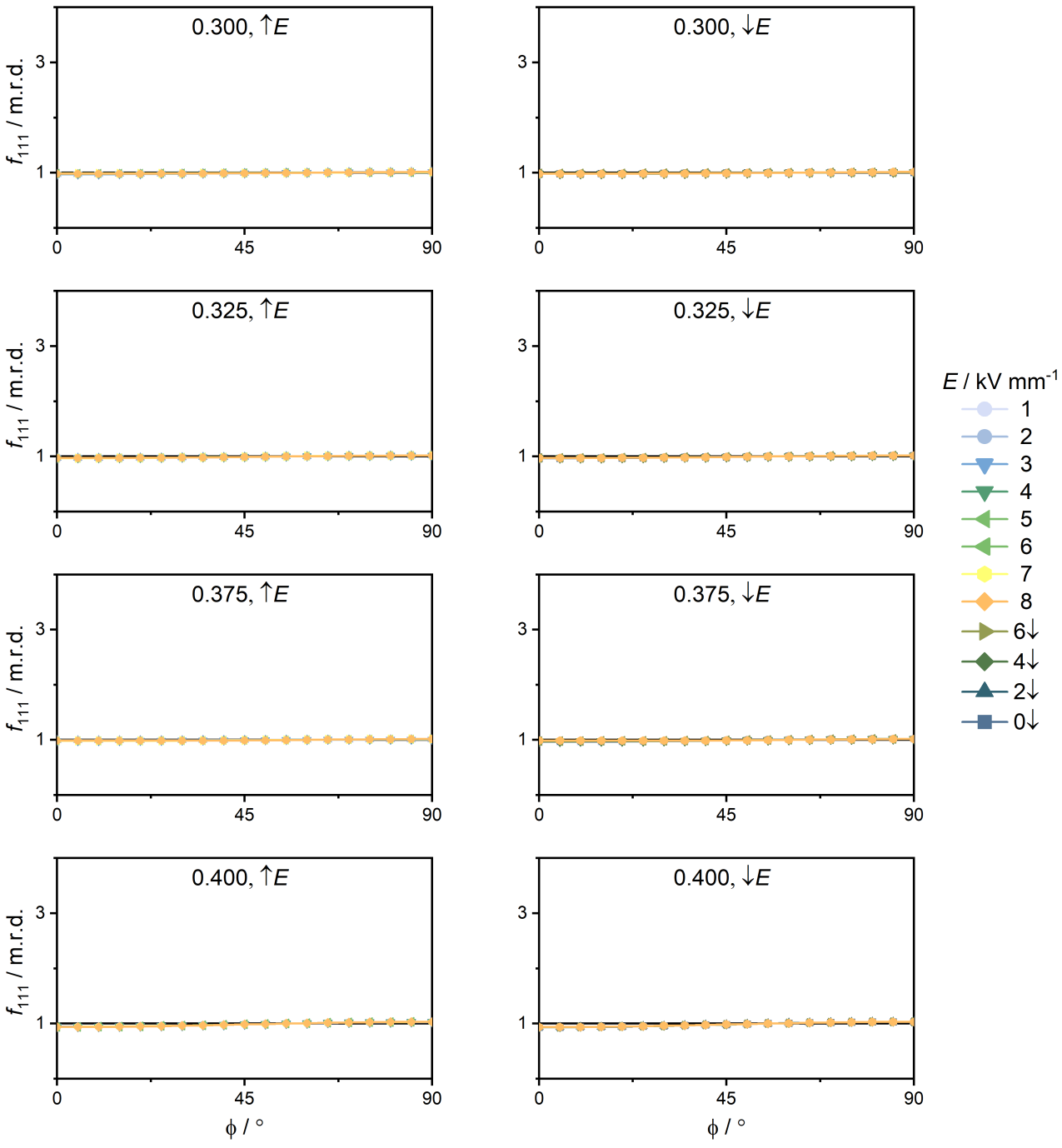

Fig. S7 Calculated 111 pole figures from the psuedocubic phase (approximated by s.g. *R*3*m*) phase in BFTM-*x*PT (*x*=0.300-0.375). Pole figures calculated from the Rietveld refinements where texture was modeled using a spherical harmonics model (order = 4)

S5 Remanent PDF data

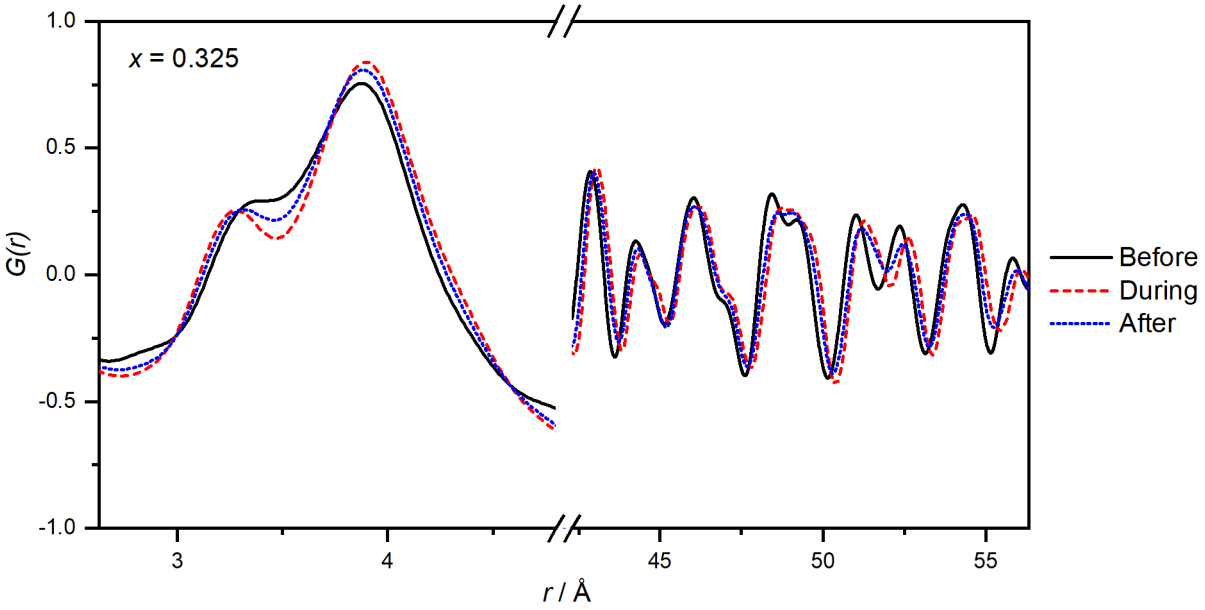

Fig. S8 PDF data collected parallel to electric field ($\phi = 0\,^{\circ}$) on $x = 0.325$ measured before, during (at $8\,\mathrm{kV\,mm^{-1}}$), and after poling

S6 Calculation of Strain

S6.1 Extrinsic

The high-field piezoelectric coefficient (d^*_{33}) originating from extrinsic domain wall motion can be calculated via eqn. S1.

$$d^*_{33} = \frac{S_{33,\text{ext}}}{E} \tag{S1}$$

where $S_{33,\text{ext}}$ is the total extrinsic strain in the sample, and E is the applied electric field. The total extrinsic strain is the sum of the extrinsic strain of all phases weighted by their phase fraction (eqn. S2)

$$S_{33,\text{ext}} = S_{33,\text{T}} \cdot \mathcal{F}_\text{T} + S_{33,\text{R}} \cdot \mathcal{F}_\text{R} \tag{S2}$$

Since there is no texture observed in the pseudocubic phase in BFTM-xPT, then $S_{33,ext}$ simplifies to eqn. S3.

$$S_{33,\text{ext}} = S_{33,\text{T}} \cdot \mathcal{F}_\text{T} \tag{S3}$$

where $S_{33,\text{T}}$ is calculated via eqn. 3, The data reported in Fig. 10 corresponds to the d^*_{33} at $E = 8\,\text{kV}\,\text{mm}^{-1}$.

S6.2 Intrinsic

The high-field piezoelectric coefficient (d^*_{33}) can be calculated from the δr gradient. By fitting the high-field region with a straight line, the resulting slope corresponds to d^*_{33}. Converting the slope's units from $\text{mm}\,\text{kV}^{-1}$ to $\text{pm}\,\text{V}^{-1}$, provides d^*_{33} in commonly used units ($1\,\text{mm}\,\text{kV}^{-1} = 10^6\,\text{pm}\,\text{V}^{-1}$). The d^*_{33} calculated here directly corresponds to the high-field piezoelectric response that originates from intrinsic effects.

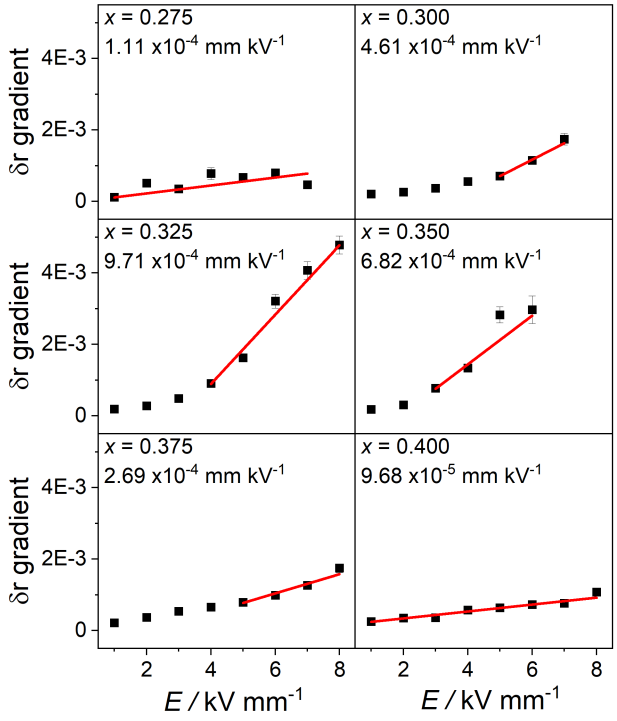

Fig. S9 δr gradient with linear fit to the high-field linear region, the slope of each fit is reported for each composition.